JOURNAL OF PROPULSION AND POWER
Vol. 26, No. 5, September–October 2010

Unstart Detection in a Simplified-Geometry Hypersonic Inlet–Isolator Flow

S. Srikant*
University of Texas at Austin, Austin, Texas 78712
J. L. Wagner†
Sandia National Laboratories, Albuquerque, New Mexico 87185
and
A. Valdivia,‡ M. R. Akella,§ and N. Clemens¶
University of Texas at Austin, Austin, Texas 78712

DOI: 10.2514/1.46937

Unstart detection techniques based on high-frequency pressure measurements made in a hypersonic inlet–isolator model are investigated. In this study, data that were acquired in a previous study of backpressure-induced unstart were examined. The data were acquired in a simplified-geometry inlet–isolator model that consisted of a 6 deg compression ramp inlet followed by a constant-area duct that was 25.4 mm high by 50.8 mm wide by 227.1 mm long. Fluctuating wall pressures were measured along the length of the model. A downstream flap was used to induce unstart in the model. Beyond a certain flap angle, unstart was induced, and the shock system propagated upstream and out of the inlet. The wall-pressure data, acquired as the flap was raised, were postprocessed for spectral and statistical content to evaluate different unstart detection criteria. Three shock leading-edge detection criteria are examined based on the following observations as the shock system passes over a pressure transducer: 1) a rise in pressure, 2) an increase in standard-deviation of the pressure signal, and 3) an increase in power in the 300–400 Hz frequency band. After calibrating the algorithms based on runs with no active control, a comparison of the times detected for unstart onset and unstart arrest was made based on runs with active control. Results indicate that the power-spectrum-based algorithm implemented close to the isolator exit is more sensitive to the onset of unstart, whereas the pressure-magnitude-change criterion gives earlier detection in many cases. A combination of the two, a pressure-magnitude criterion close to the inlet entrance and a spectral-power criterion near the isolator exit, therefore seems to be the most robust scheme for unstart active control. The appropriate choice of sampling frequency significantly improved the computation speed of the spectral-power-based algorithm without delaying the unstart detection times.

I. Introduction

SCRAMJET and ramjet propulsions are evolving technologies for hypersonic atmospheric and space vehicles. The dual-mode scramjet (DMSJ) proposed by Curran and Stull [1] is of particular interest, as it combines both scramjet and ramjet operation modes in a single flow path [2–4]. It acts as a ramjet for lower supersonic Mach numbers, transitioning to scramjet mode operation for high-supersonic and hypersonic Mach numbers. A considerable amount of research has gone into understanding and improving the performance characteristics of the DMSJ engine.

The inlet and isolator form the precombustion compression elements in a dual-mode engine [4,5]. The purpose of the isolator is to contain the shock train and prevent interaction between the combustor and inlet [4,5]. When the engine is in the ramjet mode, the pressure increases in the isolator through what is referred to as a shock train [4]. The shock train consists of a series of bifurcated normal or oblique shocks, depending on the isolator entrance conditions. Normal shock trains occur at lower entrance Mach numbers of about 2–3, while oblique shock trains are observed for higher Mach numbers [4]. The shock train allows the supersonic flow to adjust to the combustor backpressure [6].

In the presence of disturbances, such as the pressure rise due to combustion [4,5], both ramjets and scramjets have been shown to be susceptible to a highly detrimental mode of operation called unstart. Unstart can occur when the combustor backpressure is too high for the shock-train length to match. The shock system is thus disgorged from the isolator and the inlet [4]. Unstart is characterized by considerable loss in mass flow rate through the inlet, which leads to loss of engine thrust and even engine failure [4]. Unstart prevention and control is thus crucial for successful scramjet/ramjet operation.

In the flow control literature, we find several alternative strategies for unstart prevention. For example, Iannelli [7] and Chang et al. [8] have investigated mass and heat removal proportional to downstream pressure for unstart mitigation. Detection of the onset of unstart also forms an important aspect of active unstart prevention using external actuators. Rieker et al. [9] studied temperature nonuniformities in the combustor along the line of sight of a diode laser absorption sensor as a means of real-time unstart detection in a model scramjet. Their study revealed that there was a distinct increase in the low-frequency fluctuations of low-temperature gases in the combustor before the onset of backpressure-induced unstart in scramjets. Also, since unstart is characterized by the shock train being ejected out of the inlet, it is possible to detect and prevent unstart by monitoring the shock leading-edge location. Hamed and Shang [10] have shown that boundary-layer properties are significantly altered due to interaction with a normal/oblique shock wave, which results in unsteady flow when the boundary layer is separated. Carroll and Dutton [11] have confirmed this former observation, even in the absence of boundary-layer separation. Therefore, changes in wall pressure can potentially be used to detect shock leading-edge location in shock trains.

Received 31 August 2009; revision received 11 June 2010; accepted for publication 14 June 2010.

*Graduate Research Assistant, Department of Aerospace Engineering and Engineering Mechanics, 1 University Station. Student Member AIAA.
†Postdoctoral Appointee, Engineering Sciences Center. Member AIAA.
‡Graduate Research Assistant, Department of Aerospace Engineering and Engineering Mechanics, 1 University Station.
§Associate Professor, Department of Aerospace Engineering and Engineering Mechanics, 1 University Station. Associate Fellow AIAA.
¶Professor, Department of Aerospace Engineering and Engineering Mechanics, 1 University Station. Associate Fellow AIAA.

The use of time-resolved pressure measurements for shock leading-edge detection have been studied in detail by Sajben et al. [12]. They show that instantaneous axial pressure distributions and root mean square (rms) intensity amplification of pressure during shock propagation can be used to reliably estimate shock location in real time. They also proposed shock leading-edge detection by determining the upstream limit to which a search tone introduced downstream propagates. This method was largely unsuccessful in predicting shock location, except for weak shocks. Le et al. [13], however, note that the instantaneous axial-pressure-distribution-based detection recommended in [12] relies on an extensive database of inlet performance that might prove cumbersome to implement on a DMSJ for real-time shock edge detection. As plausible alternatives, Le et al. [14] proposed instantaneous pressure measurements, rms intensity [standard deviation (STD)] of pressure measurements, and spectral analysis as candidates for shock leading-edge detection. In [13], they provided easy-to-implement criteria using instantaneous wall-pressure measurements and the STD of the pressure. The performance of each criterion was analyzed on a Mach 2, hydrogen-fueled scramjet-isolator assembly, and it was observed that a criterion involving a 150% increase in the STD, relative to that upstream of the shock interaction effects, provided the quickest unstart detection. Le et al. [13] also studied spectral analysis as a means of shock detection; however, they concluded that spectral analysis did not provide earlier detection times and was more computationally intensive than the other techniques.

In this paper, we analyze fluctuating wall-pressure data to investigate schemes for detecting unstart of a simplied-geometry hypersonic inlet–isolator. The pressure data were acquired in a previous study of inlet unstart control, where an inlet–isolator model was placed on the floor of a Mach 5 wind tunnel, and unstart was initiated by deflecting a flap downstream of the isolator section [15,16]. The three different strategies tested were based on 1) pressure threshold, 2) pressure fluctuation, and 3) spectral analysis. The flow structure in this inlet–isolator model during unstart has been well characterized in previous studies with wall-pressure measurements, high-speed schlieren visualization, and particle image velocimetry (PIV) [15,17]. These studies revealed a complex and three-dimensional unstart process that was strongly associated with shock-induced separation. Furthermore, Valdivia et al. [16] and Valdivia [18] conducted a study of active control of unstart. They used real-time unstart detection based on an instantaneous wall-pressure change in the inlet section. Upon detection of the pressure increase, vortex generator (VG) jets (VGJs) were activated to prevent unstart. The active control technique had a success rate of about 50%. The primary shortcoming of the active control was that the time it took for the control to become effective was roughly the same time that it took for unstart to occur once it was detected.

The reason for the limited effectiveness of Valdivia et al. [16] in controlling unstart is not known, but it may be related to the simple unstart detection scheme that was used. In the current study, we investigate the more sophisticated unstart detection schemes mentioned previously. The spectral analysis scheme is motivated by the work of Hatlelid [19], who examined the spectra of pressure data for the Mach 5 inlet–isolator configuration, which are analyzed in the current paper, and observed a distinct frequency peak in the 300–400 Hz range near the onset of unstart. In this paper, we attempt to precisely quantify the change in spectral content for different frequency bands over time and devise specific algorithms for unstart detection based on these spectral content variations. An algorithm based on monitoring the changes in the rms pressure fluctuation in the isolator is also developed as a means to detect unstart. The unstart detection schemes described herein are compared with the real-time unstart detections of Valdivia et al. [16], which were based on a pressure-change (threshold) criterion.

II. Experimental Setup

The experimental data [16,18] that were analyzed in this study were taken in the Mach 5 blowdown wind tunnel at the University of Texas at Austin. External storage tanks with a volume of 4 m^3 (141 ft^3) were pressurized to 17.6 MPa (2550 psia) by a four-stage compressor (Worthington HB4) and were used for the air supply in each run. The stagnation pressure was 2.45 ± 0.05 MPa (355 ± 7 psia), and the stagnation temperature was 319 ± 8 K (575 ± 15 R). The freestream Mach number and velocity were 4.9 and 740 m/s, respectively [16]. The freestream turbulence intensity, as measured by PIV, is no more than 0.3% [20]. The freestream Reynolds number was 69×10^6 m^{-1} (21×10^6 ft^{-1}). The constant-area test section had a width of 152.4 mm (6 in), a height of 177.8 mm (7 in), and a length of 762 mm (30 in). Fused silica windows that were 381 mm (15 in) long and 50.8 mm (2 in) tall were placed in the test section side walls for flow visualization.

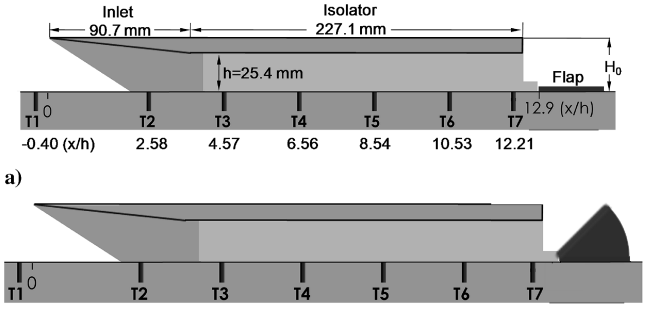

Fig. 1 Baseline inlet–isolator model: a) schematic with the portside wall removed and with the flap down and b) schematic with the flap at an angle of 45 deg.

Figure 1 shows what is termed as the baseline inlet–isolator. Figure 1a shows the model with the flap fully down, and Fig. 1b shows the model with the flap raised to 45 deg. The model consisted of a 6 deg compression ramp inlet and a constant-area isolator. The inlet–isolator assembly was floor-mounted in the test section of the wind tunnel. The coordinate system is normalized by the isolator height h. The height at the entrance of the inlet H_0 was 34.9 mm (1.35 in), and the isolator height h was 25.4 mm (1.00 in). The aspect ratios (width:height) at the inlet entrance and that of the isolator were 1.45 and 2, respectively. The inlet sidewalls were swept back 53.5 deg with respect to the y axis. A mechanical flap driven by a rack-and-pinion drive system [17] was used to simulate increases in combustor pressure. In the fully down position, the flap leading edge was at $x/h = 12.9$. Further details on the flap drive system and its control are given in [17,18].

The floor-mounted model ingested the turbulent floor boundary layer, which was thick in comparison to the inlet height. The floor boundary layer had the following properties: 99% thickness $\delta =$ 19.3 mm (0.76 in), displacement thickness $\delta^* = 8.7$ mm (0.34 in), momentum thickness $\theta = 0.77$ mm (0.030 in), and Reynolds number based on momentum thickness, $Re_\theta = 53,000$ [15]. In the baseline model, the ceiling and sidewall boundary layers developed naturally.

The tunnel floor was instrumented with transducers having an effective frequency response of about 50 kHz. The transducers (denoted T1 through T7) are shown in the schematic of Fig. 1a. Transducers T1 through T6 were slightly off center, 4.1 mm in the starboard direction, to accommodate a laser-exit window used in other experiments that used PIV. Transducer T7 was at the spanwise center of the isolator. Transducers T2 through T7 (Kulite XCQ-062-50A) had an output range of 0–350 kPa (0–50 psia), and T1 (Kulite XCQ-062-15A) was capable of measuring 0–100 kPa (0–15 psia). Wideband differential amplifiers (Dynamics model 7525) amplified the pressure signals that were then low-pass filtered at a cutoff frequency of 50 kHz using active filters (DL Instruments model 4302 or Ithaco S30). The signals were digitally sampled at 192 kHz, using two analog-to-digital converters (National Instruments data acquisition PCI-6110E) and placed in a personal computer. Further details of the pressure measurements system can be found in [17].

To achieve active control, Valdivia et al. [16] used a combination of ramp-type VGs and VGJs on the inlet sidewalls. Figure 2a shows the geometry of the ramp VGs, and Fig. 2b shows the VGs mounted

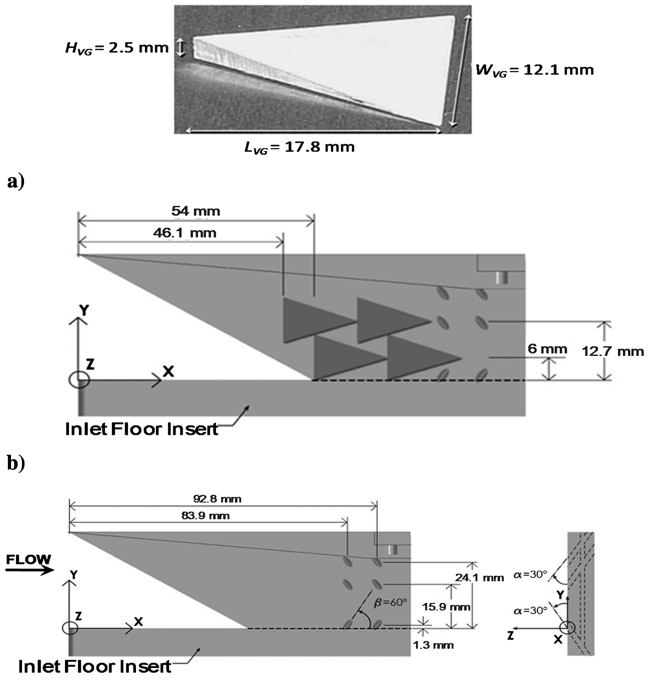

Fig. 2 Inlet flow control devices: a) a single ramp VG used for the WDs, b) WDs along the inlet sidewalls, and c) locations and orientations of the VGJs used in the active control work of Valdivia et al. [16].

along the inlet sidewalls. A configuration that uses a row of two streamwise ramp VGs is known as a Wheeler doublet (WD) configuration. Valdivia et al. [16] used the combination of WDs and VGJs, because early attempts with VGJs only showed that the VGJs would unstart the inlet when activated. However, when used in combination, the VGJs successfully stopped unstart of the inlet with WD trips [16,18]. They also showed that placing passive WDs along the inlet sidewalls greatly reduced the unsteadiness of the ramjet mode flow in the model. For example, the STD of the isolator floor pressure decreased by 58% as compared with the baseline ramjet mode flow. The WDs likely act as trips, resulting in turbulent inlet sidewall boundary layers. The locations and orientations of the VGJ ports are shown in Fig. 2c.

As described previously, the current work seeks to improve the capability to detect unstart. Toward this end, data acquired in previous unstart active control studies [16,18] are postprocessed, such that more reliable unstart detection schemes can be developed.

III. Unstart from the Ramjet Mode

The flow in the inlet–isolator responds to changes in flap position, because this changes the backpressure of the isolator. As the flow in the inlet–isolator responds to the flap, the pressures at T1–T7 respond accordingly. Figure 3 shows the pressure time histories of an inlet transducer (T2) and a transducer that is in the streamwise center of the isolator (T5) during a sequence of flap position variations in the model containing the inlet outfitted with WDs (Fig. 2b). The pressures are normalized by the freestream pressure of 5.17 ± 0.41 kPa (0.7 ± 0.06 psia). Valdivia et al. [16] provided detailed plots of the baseline (steady state) axial pressure distributions and pressure distribution as a function of the flap angle, with corresponding schlieren images, for this model. The pressure data at these transducers were used to develop the unstart detection techniques in the subsequent section of this paper. Further flowfield characterizations of this inlet–isolator are given in [16]. Figure 4 shows a sequence of schlieren images acquired during the same wind-tunnel run as in Fig. 3. The flow is from left to right, and white lines are used to denote the model walls and the flap. Details on the schlieren imaging system are given in [16,17]. At $t = 0$ in Fig. 3, the flap is in the fully down position, and the inlet–isolator flow is fully supersonic and said to be in a scramjet mode. Figure 4a shows the fully supersonic flow to consist of a series of ramp shock reflections (arrows 1–3). Note that the incident ramp oblique shock is visually obscured by the aluminum inlet section. At a time of about 0.1 s in Fig. 3, the flap is instructed to increase its angle to 43.8 deg. It takes roughly 0.3 s for the flap to get to this angle. During this time, a high-compression shock system analogous to what may be found in the ramjet mode of a DMSJ is formed. During the formation of what is called, herein, the ramjet mode shock system, the pressure increases at T5 ($x/h = 8.54$), at a time of 0.393 s, as the shock system propagates upstream across it. The schlieren image of Fig. 4b, taken at $t = 0.393$ s, shows an image of the ramjet mode shock system as it moves upstream. A floor separation shock (arrow A) originates at an x/h location of about eight. The floor separation shock impinges on the ceiling at about $x/h = 10$ and results in a reflected shock (arrow B). From 0.4 to 0.5 s, the flap is held constant at the angle of 43.8 deg. Figure 4c, taken at $t = 0.400$ s, shows the ramjet mode shock system after the flap is stable and at the angle of 43.8 deg. A ceiling separation shock (arrow C) originates at about $x/h = 6$, and a floor separation shock (arrow D) is seen at a similar streamwise location. The shocks appear to cross, resulting in a flow structure that resembles an oblique shock train [4]. Downstream of the leading separation shocks is what appears to be another pair of crossing oblique shocks (arrow E). At 0.5 s, the flap angle is increased to 44.3 deg, followed by another increase at 0.75 s to 44.7 deg. As the flap angle increases, the ramjet shock system propagates upstream, resulting in an increase in the pressure at the isolator transducer T5. At 1.0 s, the flap begins to increase its angle until about 1.05 s, where it remains at a stationary 45.1 deg until the time of 1.25 s. However, at $t = 1.142$ s, the ramjet mode shock system has propagated upstream of the inlet transducer T2 ($x/h = 2.58$). Once the inlet transducer T2 is crossed, unstart is inevitable (without control). Thus, the crossing of the inlet transducer T2 gives a reference time for the onset of unstart. Since the inlet–isolator unstarts at a stationary flap angle of 45.1 deg, the corresponding ramjet shock system is marginally stable. It is likely that perturbations, either in the freestream or floor boundary layer, induce unstart from this flow mode. Figure 4d shows a schlieren image of the marginally stable ramjet mode shock system acquired at $t = 1.094$ s. Similar to the lower-compression shock system of Fig. 4c, ceiling and floor separation shocks (arrows F and G) are observed. Owing to the highly separated flow near the floor, the point of floor separation is not clearly visualized. However, pressure measurements at T3 (not shown here) indicate that the floor separation point resides upstream of $x/h = 4.6$. Finally, at about $t = 1.146$ s, the unstart shock system crosses (not shown here) T1,

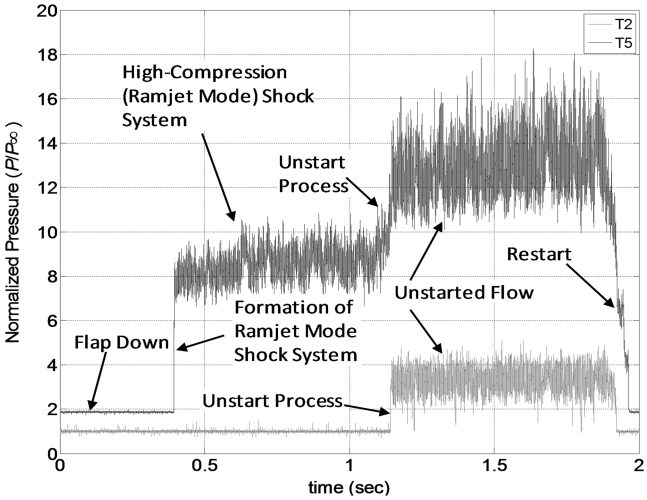

Fig. 3 Pressure time histories of the floor transducers at $x/h = 2.58$ in the inlet (T2) and at $x/h = 8.54$ in the isolator (T5) to demonstrate the ramjet mode shock system flows, the unstart process, and the unstarted flow in the inlet–isolator of Fig. 1, which is instrumented with the WDs of Fig. 2.

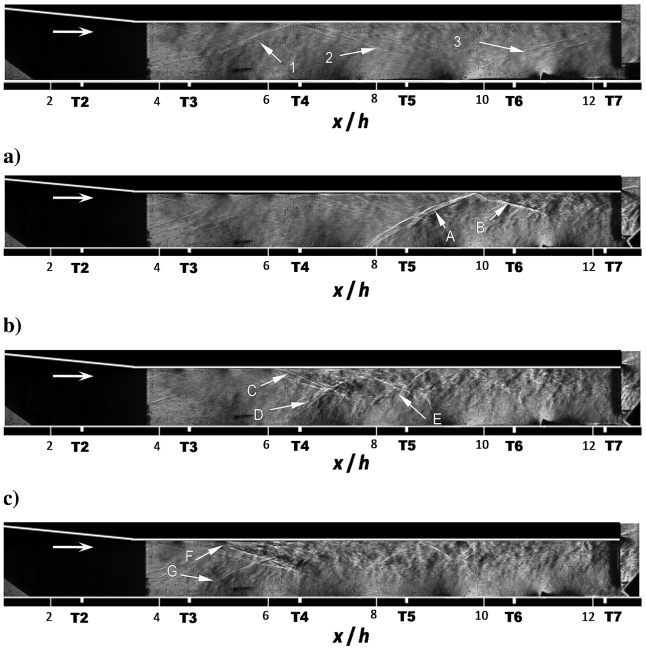

Fig. 4 Schlieren images in the isolator acquired on the same wind-tunnel run as that in Fig. 3: a) fully supersonic or scramjet mode flow acquired at $t = 0$, b) the formation of the ramjet mode shock system at a time of $t = 0.393$ s, c) the ramjet mode shock system at $t = 0.400$ s and with a stationary flap at 43.8 deg, and d) the marginally stable ramjet mode shock system at $t = 1.094$ s and with a stationary flap at 45.1 deg.

which is at $x/h = -0.4$ and thus upstream of the inlet. It is at this time that the inlet–isolator is defined to be unstarted. Figure 3 shows that the unstarted flow results in further increases in the pressures at T2 and T5.

The time it takes the shock system to propagate from the inlet transducer T2, at $x/h = 2.58$, to T1 upstream of the inlet at $x/h = -0.4$ is about 4 ms. Valdivia et al. [16] were able to actively control unstart in the current model, using VGJs and a pressure threshold detection method of the inlet transducer pressure T2. However, only a 50% unstart control success rate was achieved. This was argued to be due to the fact that the time it took for the flow control to be activated and for the flow to respond to the control was about 4 ms, which was roughly the same amount of time it took the shock system to leave the inlet once it was detected.

IV. Shock Leading-Edge Detection Techniques

The focus of our work, as mentioned previously, is to develop unstart detection algorithms based on the statistical and spectral content of the pressure signals. Specifically, algorithms are designed to detect abrupt changes in STD and spectral power in a frequency band that signify the onset of unstart. In this section, we will show a direct correlation between the STD and spectral power of pressure signals with onset of unstart and use the same to develop detection algorithms.

We use two data sets (run 404 and run 419) from [18], which have no active control implementation. These no-control cases are used to set up the algorithms and choose the parameters. In both runs, the inlet–isolator model is outfitted with WDs but no VGJs to actively prevent unstart. Further, the pressure trace from transducer T1 in both cases indicates that the shock system exits the inlet, resulting in unstart at $t = 1.0381$ s and $t = 1.1460$ s, and it restarts at $t = 1.9039$ s and $t = 1.9065$ s, respectively. The parameters and thresholds for the detection algorithms will be adjusted so as to ensure correct unstart and restart detection for these runs.

Valdivia et al. [16] implemented an instantaneous pressure-magnitude-based detection method to predict the onset of unstart. They observed that instantaneous pressure changes in transducer T2 (see Fig. 3) could be used reliably for unstart detection. This will form the baseline for comparison in the subsequent section while analyzing the efficacy of the algorithms developed in this section. The flowchart for the pressure-magnitude-based detection algorithm as implemented in real time by Valdivia et al. [16] is shown in Fig. 5. SP1 and SP2 are the lower and higher thresholds, respectively, and the window size used for unstart detection was $w_u = 10$ data points, which corresponds to about 0.05 ms.

A. Standard-Deviation-Based Detection

It is evident from Fig. 3 that the rms intensity of pressure increases in magnitude as the shock train moves upstream. To

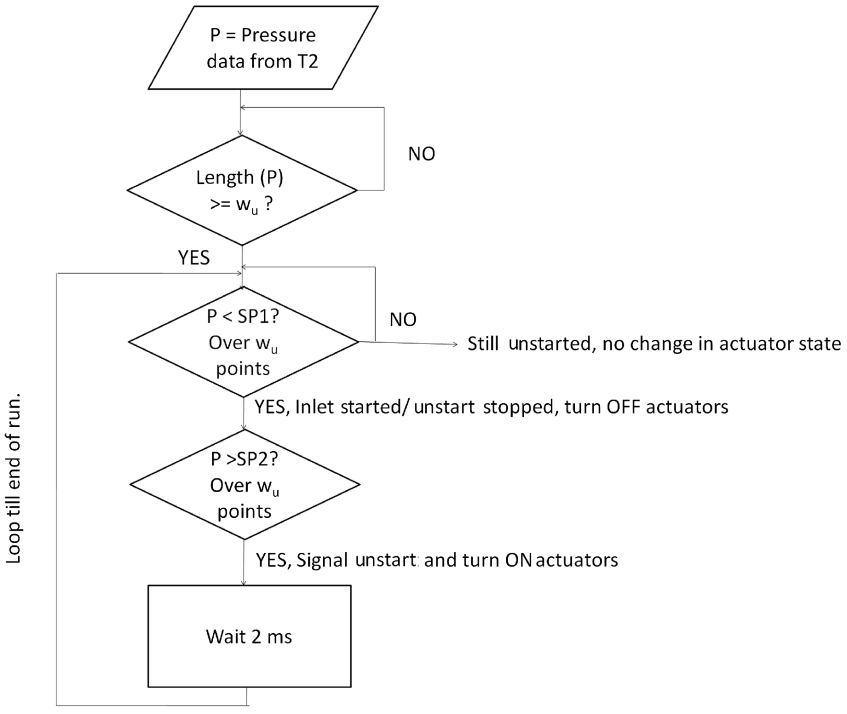

Fig. 5 Pressure-magnitude-based unstart detection; the 2 ms delay is introduced to prevent actuator burnout.

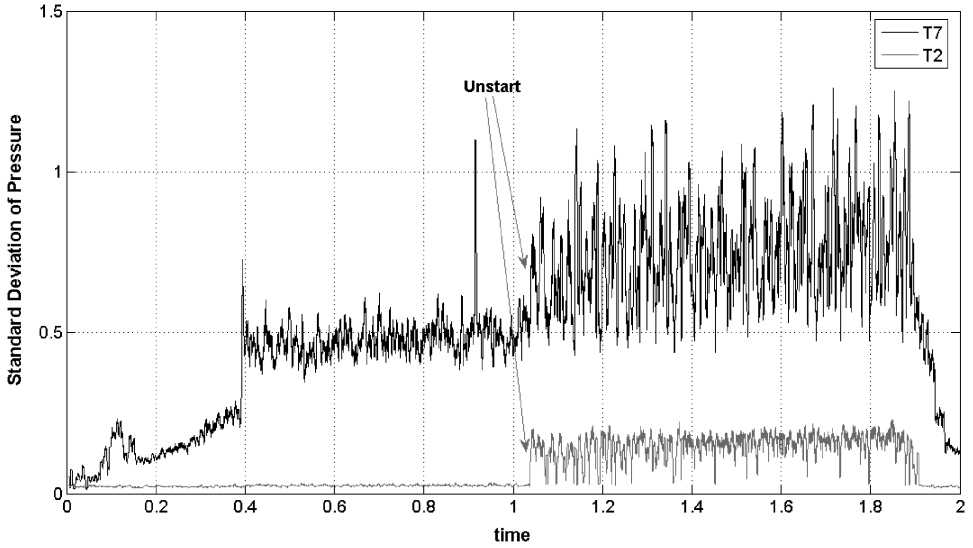

Fig. 6 STD of pressure: transducers T2 and T7.

confirm this observation, we computed the STD of the pressure data over a moving window of 4.16 ms (800 data points) for the most upstream transducer within the inlet, T1, and the most downstream transducer, T7, for the run 404. The corresponding plot is shown in Fig. 6. It is evident that either transducer shows an abrupt change in STD around the time of unstart ($t = 1.0381$ s) and decreases back on restart ($t = 1.9039$ s), which can be used for unstart detection. The flowchart for the STD-based detection algorithm is shown in Fig. 7. The different parameters required in the algorithm implementation are 1) the moving window size for computing the STD of pressure data w, 2) the maximum threshold of STD for unstart detection $h_{\max}$, 3) the minimum threshold of STD for model restart detection $h_{\min}$, and 4) the window over which comparison with the thresholds is made w_u.

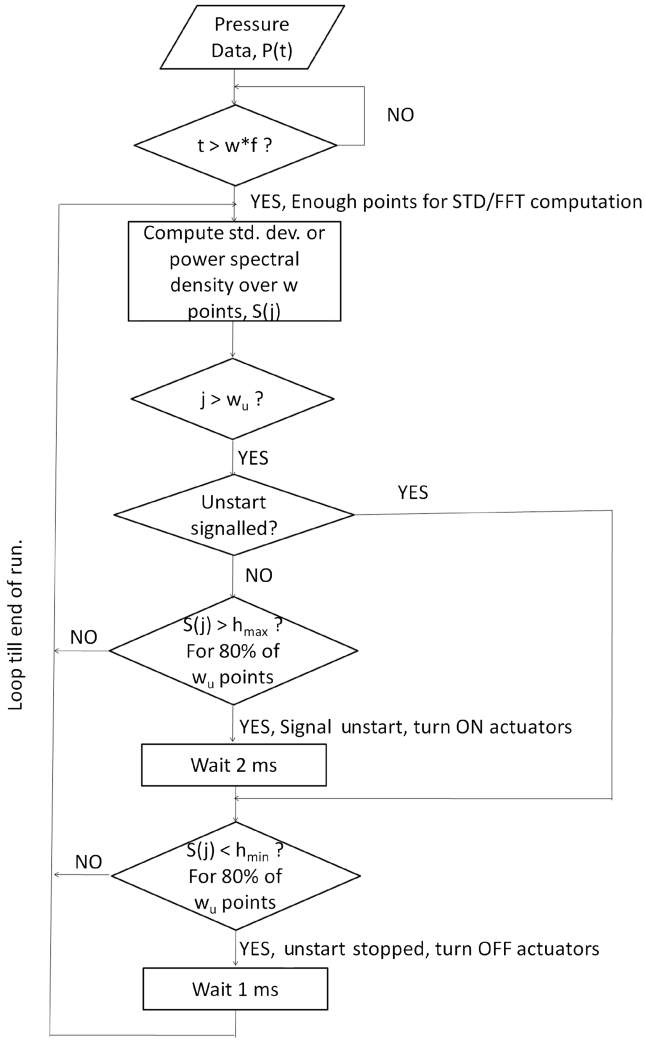

Fig. 7 Flowchart for STD-based and spectral-power-based unstart detection; f is the digital sampling frequency (192,000 kHz). The 1 ms delay after arrest of unstart signifies activation time for actuators.

It must, however, be noted that the increasing trend in transducer T7 cannot be used for detecting unstart due to the spikes, even before the onset of unstart, which lead to false detections. The first step was, therefore, to determine the transducer closest to T7 that can be reliably used for unstart detection. Based on data from runs 404 and 419, it was concluded that the most upstream isolator sensor, T3 ($x/h = 4.57$), provided the cleanest STD plots for detection of onset of unstart. To optimize the moving window size over which the STD is computed, STD of the pressure data was computed with three different window sizes, using pressure data from transducer T3. The corresponding plot is shown in Fig. 8.

It can be seen that the larger window size has, as expected, a smoothing effect in either run. We therefore choose the window size $w = 800$ data points to reduce the likelihood of false detections. The reason for experimenting only with these values of window size is that larger window sizes will lead to slower unstart detection, as sudden changes will not be properly recorded due to smoothing. It must be pointed out that the choice of the window size is likely to be specific to a particular flow configuration and data set.

Now that the choice of the pressure transducer to be used and the moving window size for computing the STD of the pressure data has been made, we proceed to choose appropriate thresholds $h_{\max}$ and $h_{\min}$. The idea behind making the choice is to ensure that the algorithm detects a single unstart and one restart for both runs 404 and 419, as we know was the case by looking at pressure data from transducer T1. To make the least conservative choice for the thresholds, we look more closely at Figs. 8c and 8f.

Figures 9a and 9b reproduce Figs. 8c and 8f, with the inset focusing on the time just before the inlet–isolator model restarted. The maximum STD on T3 before the onset of unstart was noted to be 0.1381 and 0.1662. Thus, we choose $h_{\max} = 0.170$ to be the threshold for determining if unstart has occurred. Further, once the model unstarts, the lowest value of STD occurs just before the time when the model restarts, as is evident from the plots in the inset for both cases. The restart, as shown in the plots, is located by looking for a consistent reduction in STD around the restart times for these runs known from pressure transducer T1 data. We chose $h_{\min} = 0.094$ to be the lower threshold to determine if the model has restarted after

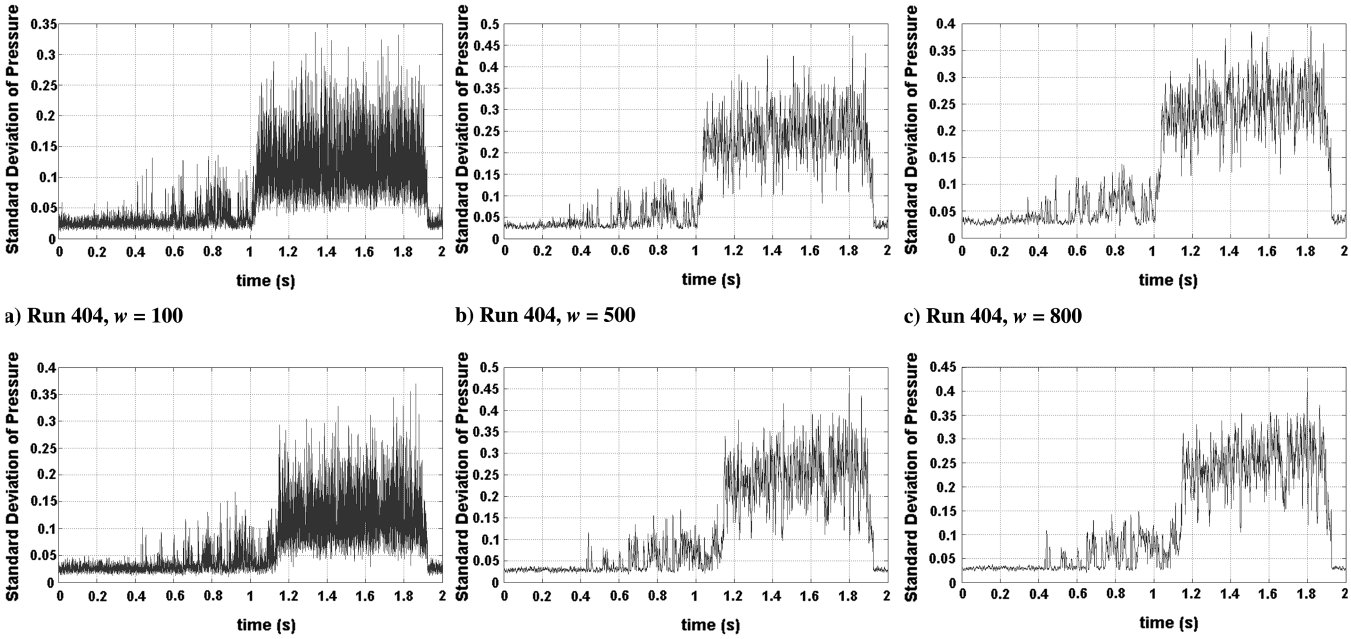

a) Run 404, w = 100 b) Run 404, w = 500 c) Run 404, w = 800

d) Run 419, w = 100 e) Run 419, w = 500 f) Run 419, w = 800

Fig. 8 STD of pressure at transducer T3 over different window sizes; $w = 100, 500, 800$.

unstart. Further, we use $w_u = 20$ to be the number of consecutive data points against which the threshold is checked. The different variable choices for setting up the algorithm have been summarized in Table 1. The algorithm, when implemented with the choice of parameters as in Table 1, for runs 404 and 419 signaled unstart at $t = 1.0379$ s and 1.1457 s, respectively, while restart was detected at $t = 1.9245$ and 1.9211 s, respectively. This is the expected result, since we know that these runs have a single unstart and restart based on transducer T1 pressure data. Thus, this represents the calibration the STD-based detection algorithm.

It must be pointed out that, although the size of the moving window w is chosen to be 800 ($\approx$4.17 ms), it is not indicative of the delay in detection, since the window moves forward by only a single sample in each iteration. It is, however, assumed that unstart does not occur in the first 4.27 ms ($w + w_u = 820$ data points).

B. Power-Spectrum-Based Detection

Power-spectrum-based detection relies on frequency-domain characteristics of the pressure measurements, as illustrated by Fig. 3. The frequency spectrum is computed using the MATLAB® discrete Fourier transform code on data sampled before and around unstart. However, the discrete Fourier transform only computes the spectral density of a static signal. To use the fast Fourier transform (FFT) as an unstart detection algorithm for dynamically sampled data, we need to monitor the changes in different frequency bands with time. This is precisely the nature of the detection algorithm we have developed, which computes the FFT over a moving window of time and monitors changes in a certain frequency band. The algorithm is similar in implementation to the STD-based algorithm, and the flowchart is as shown in Fig. 7. This technique is indeed well known in signal processing literature as the discrete-short-time Fourier transform [21,22] (DSTFT) and has been used extensively for audio signal processing.

Figure 10 represents the frequency characteristics of pressure data from run 404 recorded on transducers T2 and T4. The plot shows the energy distribution across frequencies from 0–1000 Hz in the three stages of the flow: steady (fully supersonic) flow, ramjet mode, and unstart. Figure 10a shows that transducer T2 does not experience any pressure changes due to the ramjet mode. This is to be expected since, as previously described, the ramjet mode shock system remains downstream of the inlet sensor T2. We can approximately estimate the onset of each of the ramjet and unstart modes by looking for abrupt changes in the pressure amplitude. Pressure data over a window of 0.2 s is then grabbed around this estimated time to compute the spectral density in 0–1000 Hz range for each of the flow modes. On transducer T2, located in the inlet, there is a distinct increase in all frequency ranges, although a higher change is observed in the 50–100 Hz and 300–400 Hz ranges. However, in the downstream transducers, the 300–400 Hz unstart signature is more distinct, and this frequency band shows the most marked rise in power during unstart. In contrast to transducer T2, we find that the more downstream transducer T4 shows significant spectral power in ramjet mode, which is a consequence of the strong oscillatory lambda shock structure in the isolator during the ramjet mode, as seen in Fig. 4.

The results from Fig. 10 indeed confirm the observations made by Hatlelid [19]. It must, however, be pointed out that the 300–400 Hz signature for the onset of unstart is valid only in the presence of the WDs. In runs with no WDs, the 150–200 Hz range showed the most increase in spectral power during unstart, although the trend was not as distinct as in the presence of WDs. As has been pointed out earlier, a DSTFT type algorithm developed in MATLAB is used to detect the changes in the 300–400 Hz spectrum with time in order to detect unstart.

The focus of this work is the development of an implementable algorithm based on the increase in spectral power seen in the 300–400 Hz range during unstart. With the basic algorithm now established, the next essential step is to choose the various detection parameters to be used in the algorithm implementation in real time. The parameters to be chosen are the same as in the case of the STD-based detection developed in the previous section. However, two important modifications in the analysis significantly improve performance and aid detection from the power-spectrum-based algorithm.

1. *Sampling Frequency Modification*

In our tests with arbitrary parameter values for the power-spectrum-based detection algorithm in runs 404 and 419, it was observed that the algorithm took a significantly longer time to execute as compared with the STD-based algorithm. This is expected, since computing the Fourier transform over a running window is an expensive computation relative to the STD calculation. Furthermore, since the sampling frequency involved was very high (192 kHz), the data records involved were also large, thus slowing down computation.

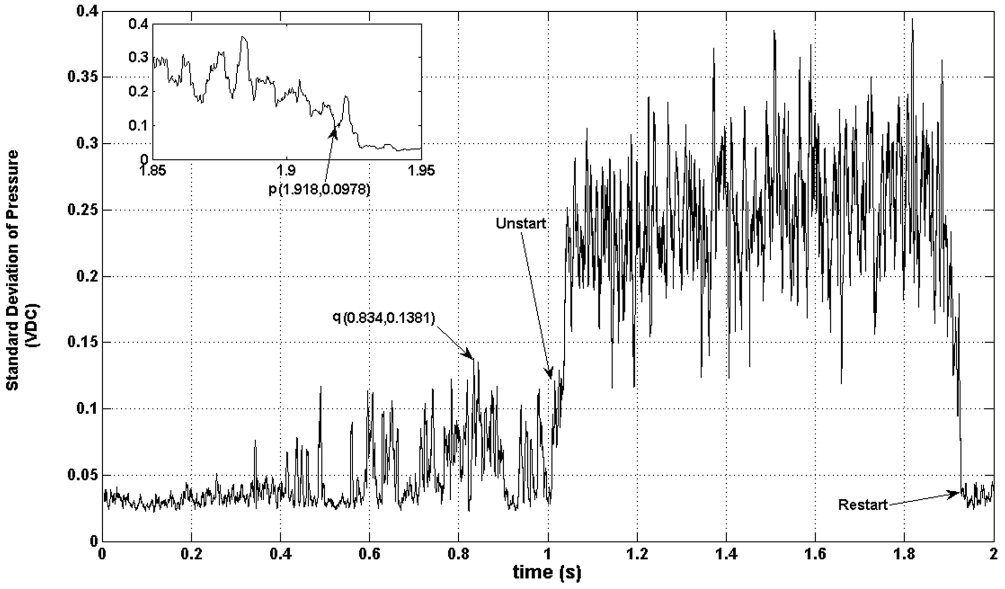

a) Run 404, w = 800

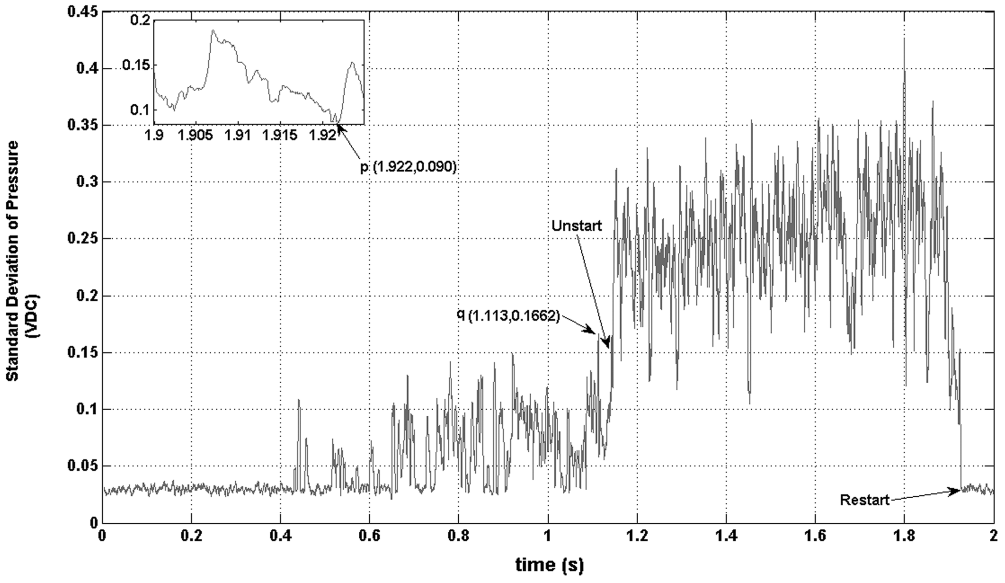

b) Run 419, w = 800

Fig. 9 STD in volts dc (VDC) vs time for runs 404 and 419, with markers displaying maximum before unstart and minimum after unstart; point p represents minimum STD after unstart, and point q represents maximum STD before unstart for these runs.

It has been pointed out earlier by Valdivia et al. [16] and Valdivia [18] that the propagation time for the shock wave was of the order of milliseconds, and the activation time for the VGJs was approximately 1 ms, which translates to a 1000 Hz frequency. We therefore observe that the digital sampling frequency from the experiments was much higher than the required accuracy for detection. For the purposes of our detection algorithm implementation, a resolution of about 0.1 ms is adequate, since it is an order of magnitude below the actuation delay and shock-propagation times. We therefore chose to artificially reduce the sampling frequency to 9600 Hz (0.104 ms/sample), as the order of magnitude of the delay introduced (0.104 ms at most) is much lower than the actuation delay. It was observed that, with this sampling frequency modification, the power-spectrum-based algorithm was as quick as the STD-based algorithm, which greatly improves the real-time implementation characteristics.

The sampling rate reduction in practice was carried out by a simple averaging over each set of 20 data points, thus reducing the effective sampling rate to $192,000/20 = 9600$ Hz. It must be pointed out that the Nyquist frequency corresponding to this sampling rate is 4800 Hz, which is much greater than the frequency band of interest (300–400 Hz). Therefore, the choice of sampling frequency made here does not introduce any aliasing issues into the spectral analysis.

Table 1 Parameter selection for STD-based unstart detection

Parameter	Value
Pressure transducer	T3
Window size, w	800 points $\approx$ 4.17 ms
Threshold, $h_{\max}$	0.170
Threshold, $h_{\min}$	0.094
Unstart detection window, w_u	20 points

2. *Fourier Transform Length Modification*

The plot for the spectral content in transducer T4 during steady, ramjet, and unstart flow modes, shown in Fig. 10b, used a window size of 0.2 s, as mentioned earlier. However, for the purposes of the moving window size w, 0.2 s is too large to allow the algorithm to be sufficiently sensitive to changes in the 300–400 Hz frequency over time. We must clarify that 0.2 s does not represent the actual detection

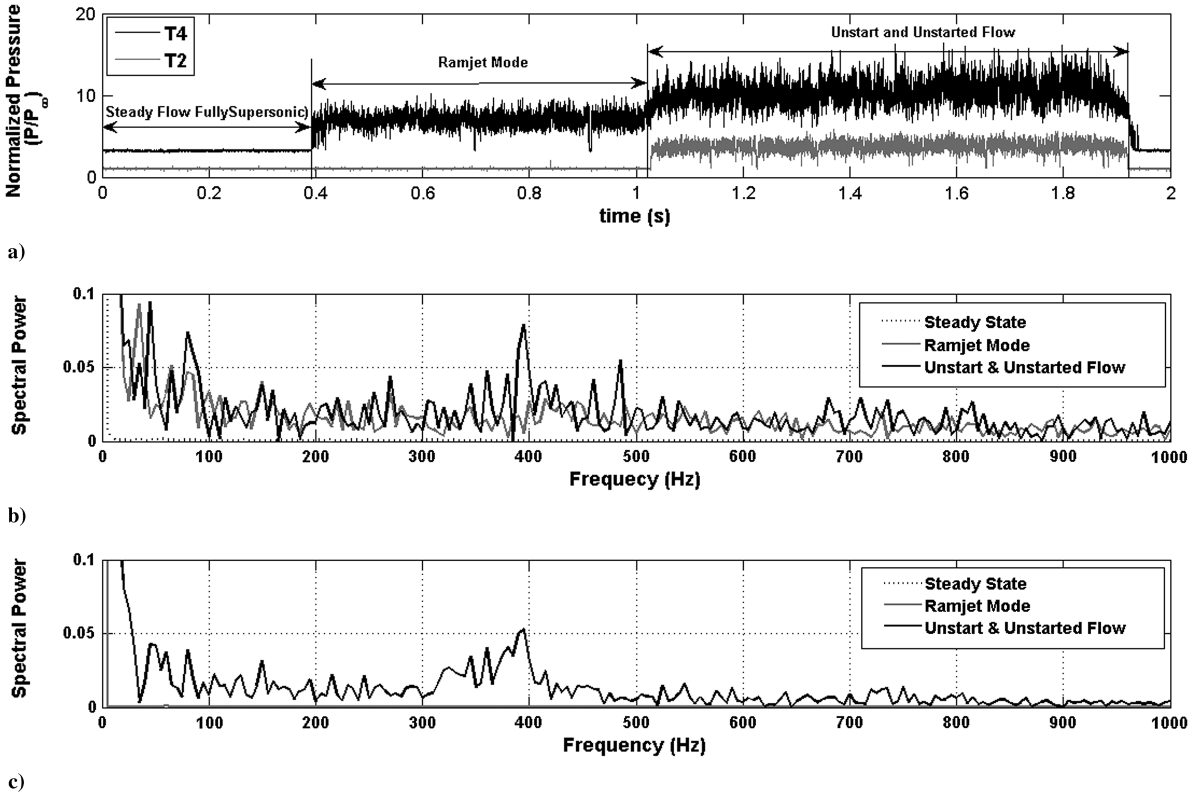

Fig. 10 Pressure data and power spectrum for run 404: a) normalized pressure, b) spectral power for T4 over 0–1000 Hz, and c) spectral power for T2 over 0–1000 Hz.

delay, because the moving window advances by only one data point (in this case, 0.104 ms corresponding to 9600 Hz sampling frequency). However, the algorithm compares the mean power in the 300–400 Hz range across different time windows. Therefore, a larger window size implies slower detection of an increase, or decrease, in spectral power.

We would therefore like to implement a smaller window size. However, this is not possible with the raw data alone, as is illustrated by Fig. 11. The figure shows the spectral-power distribution for run 404 during steady, ramjet, and unstart modes on transducer T4. We have used a window size of 0.01 s and recreated the plot shown in Fig. 10b. It is evident from this plot that, for this window size, we do not detect the increase in the 300–400 Hz frequency band. The transducers T4 through T7 were found to be very sensitive to the size of the window used for the Fourier transform computation, while not much change was detected in the transducers upstream (T1–T3).

This phenomenon is explained by the fact that the frequency resolution of the Fourier transform is inversely proportional to the number of points used to compute the Fourier transform; that is, for sampling frequency f and number of data points n (corresponding to window size w), the frequency resolution is f/n. Therefore, we need more data points (large n) to compute the frequency spectrum accurately.

This is contradictory to the requirement of a small window size to ensure quicker detection of changes in the spectral power during unstart and inlet restart. To mitigate this problem, we compute the Fourier transform of a smaller sample set ($w = 650$ points $= 0.07$ s) and artificially increase the length by padding this with an arbitrary

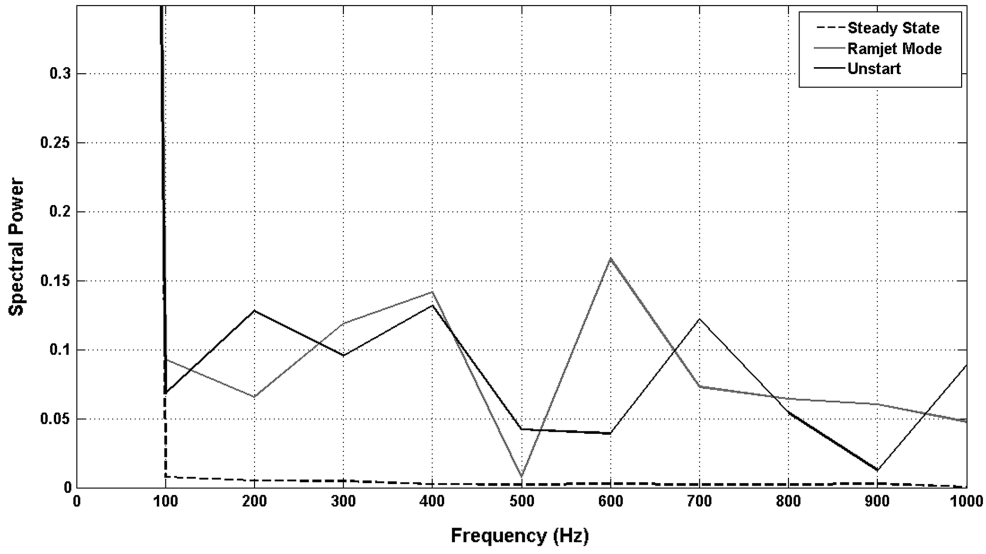

Fig. 11 Spectral power for T4 over 0–1000 Hz, using window size 0.01 s.

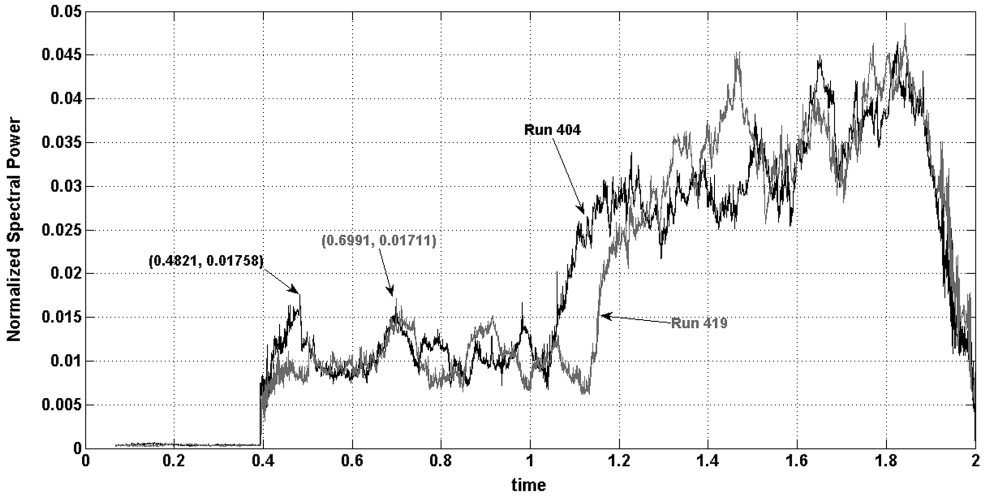

Fig. 12 Spectral-power plot for runs 404 and 419, with markers displaying maximum before unstart.

signal of known frequency. The length of the Fourier transform was chosen to be 1920 data points, which corresponds to 0.2 s at 9600 Hz sampling frequency. Since the signal was padded uniformly over each window of time with the same padding signal, the frequency of the padding signal was of no significance. Therefore, we chose to use the simplest possible padding signal [i.e., a dc (constant) signal].

The choice of window size as mentioned above corresponds to transducer T4, which is what we shall use for detection purposes. We were able to observe distinct changes in spectral power over the 300–400 Hz range for all transducers during unstart; however, further downstream, transducers did not yield any improvement in detection times due to higher pressure fluctuations that existed closer to the isolator exit. We also chose the size of the unstart detection window $w_u = 5$ data points ($\approx$0.52 ms based on 9600 Hz sampling rate). The choice of thresholds, as in the case of the STD-based detection, is calibrated based on runs 404 and 419. We choose the lowest $h_{\max}$ and largest $h_{\min}$ to ensure there was a single unstart and single restart event detected for each run, as is known from transducer T1 pressure data.

Figure 12 shows the normalized spectral power as computed for runs 404 and 419 on transducer T4 with the previously specified window size. On the plot are marked the maximum values of the spectral power for each run before the onset of unstart. Based on these values, we made a choice of $h_{\max} = 0.0175$. Further, as was the case for Fig. 9, the least values of spectral power beyond unstart were observed just before restart (near the 2 s mark). Based on spectral-power values before restart, $h_{\min}$ was chosen to be 0.012. The parameter values for the power-spectrum-based unstart detection algorithm are summarized in Table 2. The algorithm implemented with the parameter values in Table 2 on runs 404 and 419 detected unstart at $t = 1.0605$ s and $t = 1.1573$ s, and inlet restart was detected at $t = 1.9503$ s and $t = 1.9847$ s, respectively.

It must again be pointed out that, although the size of the moving window w is chosen to be 650 points ($\approx$0.068 s), it is not indicative of the delay in detection. The window moves forward by only a single sample in each iteration. It is, however, assumed that unstart does not occur in the first 0.0682 s ($w + w_u = 655$ points) of each run. We note that the power-spectrum-based algorithm as described has the potential of being implemented in practice, using an analog bandpass filter instead of a Fourier transform. However, the authors have not studied the phase lag and other filtering associated delays in this work.

Table 2 Parameter selection for power-spectrum-based unstart detection

Parameter	Value
Pressure transducer	T4
Sampling rate	9600 Hz
Window size, w	650 points $\approx$ 0.068 s
Padded window size	1920 points (0.2 s)
Threshold, $h_{\max}$	0.0175
Threshold, $h_{\min}$	0.012
Unstart detection window, w_u	5 points

V. Results

The STD and power-spectrum-based unstart detection algorithms calibrated in the preceding section were evaluated on runs 427, 430, 433, 435, 436 [18], in which pressure data were digitally sampled for a period of 2 s at 192 kHz. These runs were chosen for their similarity with runs 404 and 419, in the sense that both were equipped with WDs. Furthermore, Valdivia et al. [16] and Valdivia [18] implemented active control, using VGJs in these runs, which used the pressure-magnitude-based algorithm for unstart detection in real time. Thus, we were be able to compare results from the three different detection algorithms on each of these runs. As has been clarified earlier, the results here are based on postprocessing data collected by Valdivia et al. [16] and Valdivia [18]; however, the algorithms are implemented so as to mimic a real-time application (pressure data are fed in real time to each algorithm), and so comparison with pressure-magnitude-based detection results is justified.

The unstart detection times for each of the runs have been plotted and are being presented here for comparison. A nonzero on the plots indicates an onset of unstart signaled by the algorithms, while a zero implies unstart is not detected (active control actuators turned off). The results for the pressure-magnitude-based detection have been plotted here for reference [18]. Figure 13 shows the times at which onset of unstart and arrest of unstart were signaled by each of the three detection algorithms for run 427. The active control (VGJs) was able to prevent unstart for this run, as is indicated by the fact that the pressure amplitude detection algorithm turns off the VGJs just before 2 s and does not signal an onset of unstart after that. The STD-based detection is unable to detect any onset of unstart during the entire run. The pressure-magnitude criterion has two unstart detections in quick succession between 0.7–0.8 s. The spectral-power-based criterion also detects a single unstart around this time, but the detection is delayed. However, it is important to note that the spectral-power-based algorithm indicates longer control actuation time as compared with the pressure amplitude detection method. The next detection from the pressure-magnitude criterion is at 1.938 s, which is not detected by the spectral-power-based method. The spectral-power-based criterion has two more detections in between at 1.2392 and 1.6115 s. The fact that there was no active control in the 1.2392–1.3123 s and 1.6115–1.6784 s time band, and yet no unstart occurred in the inlet (as evident from pressure data), indicates that these detections from the FFT-based algorithm were false detections.

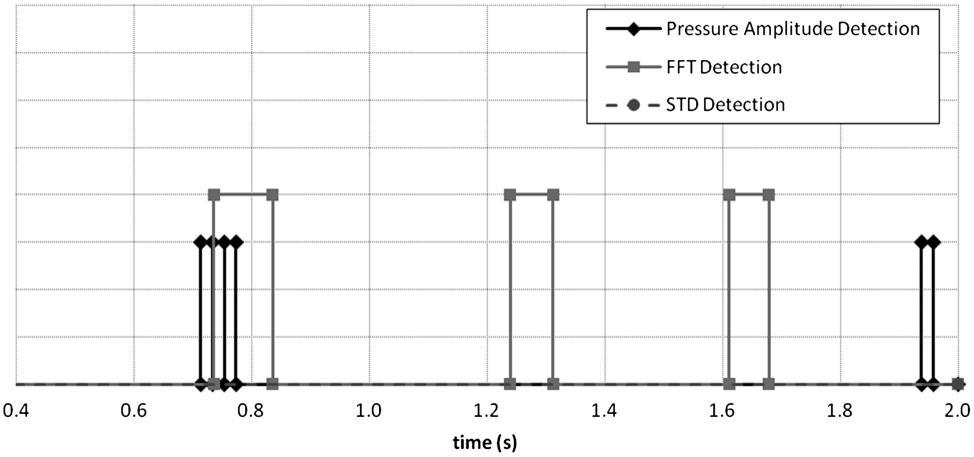

Fig. 13 Unstart detection times for run 427. A zero indicates no unstart detected and a nonzero indicates unstart detected, from pressure-magnitude criterion on T2, STD criterion on T3, and spectral-power criterion on T4.

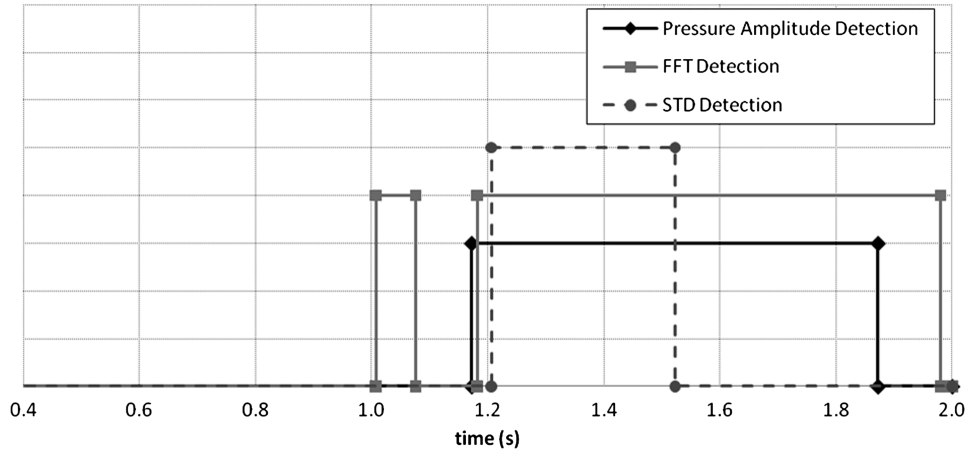

Fig. 14 Unstart detection times for run 430, 0 indicates no unstart detected and a nonzero indicates unstart detected from pressure-magnitude criterion on T2, STD criterion on T3 and spectral-power criterion on T4.

Figure 14 plots the onset of unstart and arrest of unstart times for run 430. Again, it is evident from the plot for the pressure-magnitude-based detection algorithms that unstart was successfully prevented by the active control (algorithm signals arrest of unstart before 2 s with no further unstart detection). However, as observed in Fig. 13, we find that the spectral-power-based method detects an additional onset of unstart between 1.0074–1.0763 s, which is again a false detection, as was observed in Fig. 13. The pressure-magnitude criterion detects the next onset, the earliest at 1.172 s, whereas the spectral-power method detects it at 1.1818 s and the STD method at 1.2063 s. The STD detection method also detects arrest of unstart much sooner than the other two criteria. The delayed detection of unstart and early unstart arrest signal by the STD-based detection, coupled with no unstart detections in run 427 (Fig. 13), indicates that the STD method is not sensitive enough to small changes in the pressure, which might eventually lead to unstart if uncontrolled. This pattern in unstart detection from the STD-based algorithm is observed in all subsequent runs. We again observe for this run that the

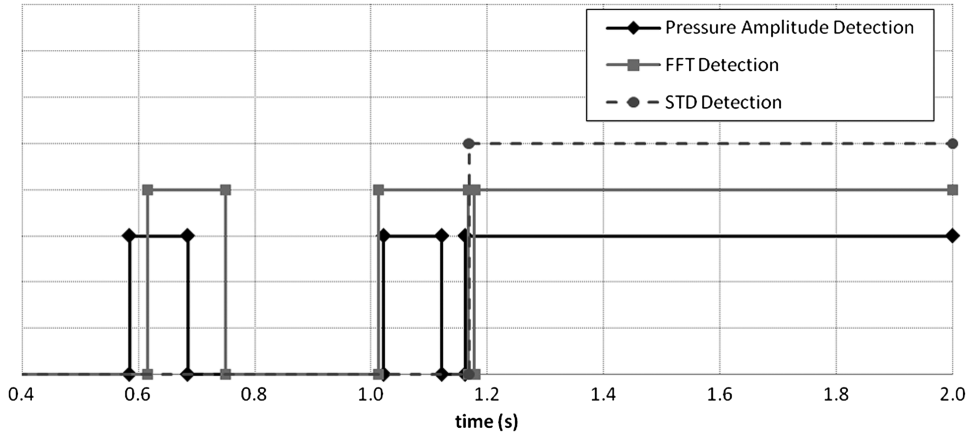

Fig. 15 Unstart detection times for run 433. A zero indicates no unstart detected and a nonzero indicates unstart detected from pressure-magnitude criterion on T2, STD criterion on T3, and spectral-power criterion on T4.

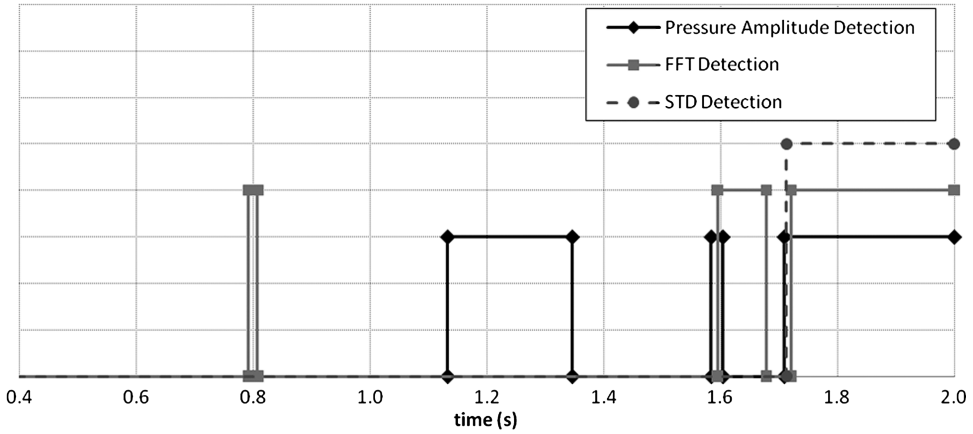

Fig. 16 Unstart detection times for run 435. A zero indicates no unstart detected and a nonzero indicates unstart detected from pressure-magnitude criterion on T2, STD criterion on T3, and spectral-power criterion on T4.

spectral-power criterion would ensure longer control actuation, as in run 427.

Figure 15 shows the unstart detection results for run 433. This is different from the last two cases, because the active control (VGJs) were unable to prevent the inlet from unstarting. The STD method does not provide any additional information, other than a single unstart detection at 1.1682 s. The pressure-magnitude criterion detects an early onset of unstart at 0.5847 s, whereas the spectral-power method detects the same at 0.6162 s. The spectral-power method commands longer control actuation as before (0.1336 s from spectral-power method compared with 0.1001 s from pressure-magnitude-based method). The second onset of unstart is detected earlier at 1.0131 s by the spectral-power method, while the pressure-magnitude criterion detects it at 1.022 s. Furthermore, the spectral method also recommends longer control actuation up to 1.1668 s, as compared with 1.122 s by the pressure amplitude method. This additional control actuation would have been helpful in preventing the model from unstarting eventually. The last onset of unstart detection is, however, delayed when using the spectral-power method.

The next run used in the analysis is another case where the active control with VGJs was unable to prevent unstart in the model. The plot for the detection times for this run is shown in Fig. 16. Proceeding from the left to right on the plot, we observe that the spectral-power criterion detects onset of unstart between 0.7916–0.8074 s, followed by the pressure-magnitude criterion detecting onset of unstart between 1.1326–1.3460 s. However, at 1.5840 s, the pressure-magnitude criterion detects an onset of unstart, whereas the spectral-power method is slightly delayed with detection at 1.5946 s. The spectral-power method, however, signals arrest of unstart much later than the pressure-magnitude criterion, which again could eventually be the difference between a started and unstarted model. For the final event near 1.65 s, the earliest unstart detection is provided by the pressure amplitude method followed by the STD criterion and then the spectral-power criterion.

The plot of detection times for run 436 are shown in Fig. 17. Again, this is an example of an experiment in which eventual unstart of the model was not successfully arrested by the VGJs. An analysis of the plot shows that a false onset of unstart is detected at 0.6483 s by the spectral-power criterion on transducer T4. The pressure amplitude method detects the next onset earlier than the spectral-power method at 0.9531 s but, while the pressure amplitude method indicates arrest of unstart at 1.1330 s, the spectral-power method signals unstart at 0.9799 s and no subsequent arrest of unstart. The pressure amplitude method thus turns off active control at 1.1330 s and turns it back on only at 1.1990 s, beyond which they remain unable to prevent unstart, while the spectral method commands the VGJs stay on beyond 0.9799 s, enabling better unstart prevention. The STD method detects a single onset of unstart at 1.2086 s, with no subsequent detections.

In summary, based on the observations of onset and arrest of unstart detection times from each algorithm, we found the following.

1) The STD algorithm was seen to have poor sensitivity to onset of unstart. It missed most instances of unstart onset detected by the pressure-magnitude criterion and recognized only pressure changes occurring over significantly longer time spans.

2) The pressure-magnitude criterion gave earlier unstart detection in most cases. On the other hand, the criterion also declared arrest of unstart much quicker than the spectral-power-based technique.

3) The spectral-power method gave earlier detection on some runs. Also, it was observed that the arrest of unstart (and therefore VGJs off) signal was later as compared with the pressure-magnitude

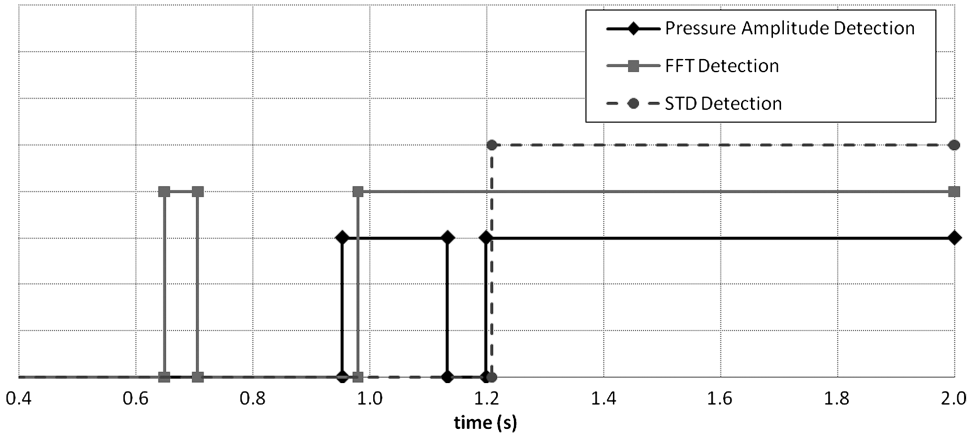

Fig. 17 Unstart detection times for run 436. A zero indicates no unstart detected and a nonzero indicates unstart detected from pressure-magnitude criterion on T2, STD criterion on T3, and spectral-power criterion on T4.

criterion. Some earlier detections and significantly longer control actuation could prove crucial in preventing model unstart, as seen in runs 433. 435 and 436.

4) The spectral-power method shows some false detections of unstart in the runs evaluated. The active control (VGJs plus WDs), however, does not induce unstart, as shown in [16,18]. Therefore, additional detections are not detrimental to inlet operation. In other words, it is probably beneficial to have false positives for unstart onset as opposed to false negatives.

Observing the detection time trends from different criteria in experimental runs, we believe that a combination of pressure-magnitude-based detection algorithm on T2 and a spectral-power-based detection algorithm on T4 will provide a significantly improved and robust unstart detection technique for this flow configuration. The idea would be to command the active control actuators (say VGJs) based on unstart onset and arrest times from each individual algorithm. The actuators are commanded to turn on when either one of the algorithms detects an onset of unstart and, subsequently, turned off when both pressure-magnitude and spectral-power criteria signal arrest of unstart. This will combine the early detection properties of the pressure-magnitude-based detection with the sensitivity of the spectral-power-based detection method.

VI. Conclusions

The efficacy of three unstart detection techniques was investigated in a postprocessing study of previously obtained experimental data. The techniques were based on high-frequency pressure measurements at a sampling frequency of 192 kHz. Wall-pressure data were analyzed that were collected in an inlet–isolator model with a downstream flap to initiate unstart. Two unstart detection algorithms based on change in STD of pressure and spectral content of the pressure signal during unstart were developed and compared against a previously developed pressure-magnitude-based detection criterion.

The pressure-magnitude and the pressure STD-based algorithms were found to not be amenable for unstart detection when using downstream locations, whereas the spectral-power-based algorithm was applicable to all locations. The ability to implement the spectral-power-based algorithm on all transducers is advantageous in developing generic detection strategies using pressure data from all axial locations for different inlet–isolator models and flow regimes. The 300–400 Hz unstart signature shown in previous studies was found to be prominent only in the downstream transducers (T4–T7), while all frequencies were seen to increase during unstart at transducers upstream of T4. The spectral-power method was thus implemented on transducer T4 data to capture this increase in the 300–400 Hz range. Modifications in the sampling rate and length of the Fourier transform improved the speed of execution of the algorithm, aiding real-time implementation, and provided better detection times. The power-spectrum-based algorithm also has the potential of being implemented using an analog bandpass filter in real experiments with much improved execution speeds. The execution time for the pressure-magnitude-based algorithm was the lowest, while the STD and spectral-power-based algorithms had similar execution times.

The algorithms were compared on pressure data previously collected from runs in which active control was implemented. It was found that the STD-based algorithm had low sensitivity to unstart detection and was not a feasible option for active control of unstart. The pressure-magnitude-based criterion, which was actually implemented in a closed-loop control scheme, has been previously shown to have a 50% success rate. It was found, by observing onset and arrest of unstart times from various runs, especially ones where the model eventually unstarted, that the pressure-magnitude-based method had smaller control actuation windows relative to the spectral-power-based algorithm. Also, the spectral-power-based algorithm detected onset of unstart earlier in some cases, which combined with longer actuation is crucial in runs where the pressure-magnitude criterion failed to prevent unstart. The spectral-power method, however, shows some false detections of onset of unstart on most runs, and so actuation would be commanded when it was not needed.

Based on the observations made in analyzing data from these experimental runs, we conclude that the pressure-magnitude-based detection algorithm implemented on upstream transducer T2 could be augmented with the spectral-power-based algorithm on transducer T4. In other words, the set of onset and arrest of unstart detection times from the pressure-magnitude-based and the spectral-power-based detection criteria should be combined and their union used to turn on or off the active control actuators. This will combine the speed of the pressure-magnitude-based method and sensitivity of the spectral-power-based method to give a more robust scheme for unstart prevention in the hypersonic inlet–isolator model.

Acknowledgments

The research work was supported in part by the U.S. Air Force Office of Scientific Research under the Multidisciplinary University Research Initiative grant FA9550-04-1-0387. The authors would also like to acknowledge the help provided by K. Bulent Yuceil at the Flowfield Imaging Laboratory, University of Texas at Austin.

References

[1] Curran, E., and Stull, F., "The Utilization of Supersonic Combustion Ramjet Systems at Low Mach Numbers," Air Force Aero Propulsion Lab., RTD-TDR-63-4097, Wright-Patterson AFB, OH, Jan. 1964.

[2] Billig, F., "Research on Supersonic Combustion," *Journal of Propulsion and Power*, Vol. 9, No. 4, 1993, pp. 499–514. doi:10.2514/3.23652

[3] Cockrell, C., Auslender, A., Guy, R., McClinton, C., and Welch, S., "Technology Roadmap for Dual-Mode Scramjet Propulsion to Support Space-Access Vision Vehicle Development," 11th AIAA/AAAF Inter. Space Planes and Hypersonic Systems and Technologies Conference, AIAA Paper 2002-5188, 2002.

[4] Heiser, W., and Pratt, D., *Hypersonic Airbreathing Propulsion*, AIAA, Washington, D.C., 1994.

[5] Curran, E., Heiser, W., and Pratt, D., "Fluid Phenomena in Scramjet Combustion Systems," *Annual Review of Fluid Mechanics*, Vol. 28, No. 1, 1996, pp. 323–360. doi:10.1146/annurev.fl.28.010196.001543

[6] Waltrup, P., and Billig, F., "Structure of Shock Waves in Cylindrical Ducts," *AIAA Journal*, Vol. 11, No. 10, 1973, pp. 1404–1408. doi:10.2514/3.50600

[7] Iannelli, J., "A Distributed Wall Mass Removal System for Improving Scramjet Isolator Performance," 46th AIAA Aerospace Sciences Meeting and Exhibit, AIAA Paper 2008-0065, 2008.

[8] Chang, J., Bao, W., Yu, D., Fan, Y., and Shen, Y., "Effects of Wall Cooling on Performance Parameters of Hypersonic Inlets," *Acta Astronautica*, Vol. 65, Nos. 3–4, 2009, pp. 467–476. doi:10.1016/j.actaastro.2009.02.005

[9] Rieker, G., Jeffries, J., Hanson, R., Mathur, T., Gruber, M., and Carter, C., "Diode Laser-Based Detection of Combustor Instabilities with Application to a Scramjet Engine," *Proceedings of the Combustion Institute*, Vol. 32, No. 1, 2009, pp. 831–838. doi:10.1016/j.proci.2008.06.114

[10] Hamed, A., and Shang, J., "Survey of Validation Data Base for Shockwave Boundary-Layer Interactions in Supersonic Inlets," *Journal of Propulsion and Power*, Vol. 7, No. 4, 1991, pp. 617–625. doi:10.2514/3.23370

[11] Carroll, B., and Dutton, J., "Turbulence Phenomena in a Multiple Normal Shock Wave/Turbulent Boundary-Layer Interaction," *AIAA Journal*, Vol. 30, No. 1, 1992, pp. 43–48. doi:10.2514/3.10880

[12] Sajben, M., Donovan, J., and Morris, M., "Experimental Investigation of Terminal Shock Sensors for Mixed-Compression Inlets," *Journal of Propulsion and Power*, Vol. 8, No. 1, 1992, pp. 168–174. doi:10.2514/3.23457

[13] Le, D., Goyne, C., and Krauss, R., "Shock Train Leading-Edge Detection in a Dual-Mode Scramjet," *Journal of Propulsion and Power*, Vol. 24, No. 5, 2008, pp. 1035–1041.doi: 10.2514/1.32592

[14] Le, D., Goyne, C., Krauss, R., and McDaniel, J., "Experimental Study of a Dual-Mode Scramjet Isolator," *Journal of Propulsion and Power*, Vol. 24, No. 5, 2008, pp. 1050–1057.doi: 10.2514/1.32591

[15] Wagner, J. L., Yuceil, K. B., and Clemens, N. T., "PIV Measurements of Unstart of an Inlet–Isolator Model in a Mach 5 Flow," *AIAA Journal* (accepted for publication).

[16] Valdivia, A., Yuceil, K. B., Wagner, J. L., Clemens, N. T., and Dolling, D. S., "Active Control of Supersonic Inlet Unstart Using Vortex Generator Jets," 39th AIAA Fluid Dynamics Conference, AIAA Paper 2009-4022, June 2009.

[17] Wagner, J., Yuceil, K., Valdivia, A., Clemens, N., and Dolling, D., "Experimental Investigation of Unstart in an Inlet/Isolator Model in Mach 5 Flow," *AIAA Journal*, Vol. 47, No. 6, June 2009, pp. 1528–1542. doi:10.2514/1.40966

[18] Valdivia, A., "Active Control of Supersonic Inlet Unstart Using Vortex Generator Jets and Wheeler Doublet Vortex Generators," M.S. Thesis, Univ. of Texas, Austin, TX, May 2008.

[19] Hatlelid, J. A., "Active Control to Prevent Inlet Unstart," M.S. Thesis, Univ. of Texas, Austin, TX, Aug. 2008.

[20] Wagner, J. L., "Experimental Studies of Unstart Dynamics in Inlet/Isolator Configurations in a Mach 5 Flow," Ph.D. Thesis, Department of Aerospace Engineering and Engineering Mechanics, Univ. of Texas, Austin, TX, 2009.

[21] Allen, J., "Short Term Spectral Analysis, Synthesis, and Modification by Discrete Fourier Transform," *IEEE Transactions on Acoustics, Speech, and Signal Processing*, Vol. 25, No. 3, 1977, pp. 235–238. doi:10.1109/TASSP.1977.1162950

[22] Allen, J., and Rabiner, L., "A Unified Approach to Short-Time Fourier Analysis and Synthesis," *Proceedings of the IEEE*, Vol. 65, No. 11, 1977, pp. 1558–1564. doi:10.1109/PROC.1977.10770

C. Segal
Associate Editor